JOURNAL OF MATERIALS SCIENCE **36** (2001) 3707–3714

Microstructure and tensile properties of *in situ* synthesized (TiB_w + TiC_p)/Ti6242 composites

WEIJIE LU, DI ZHANG, XIAONONG ZHANG, YUJUN BIAN, RENJIE WU
State Key Laboratory of Metal Matrix Composites, Shanghai Jiao Tong University, 200030, Shanghai, People's Republic of China
E-mail: lvweijie@yahoo.com

T. SAKATA, H. MORI
Research Center for Ultra-High Voltage Electron Microscopy, Osaka University, Yamadaoka, Suita, Osaka 565-0871, Japan

In the present work, ($TiB_w + TiC_p$)/Ti6242 composites were fabricated via common casting and hot-forging technology utilizing the SHS reaction between titanium and B_4C. The XRD technique was used to identify the phases of composites. The microstructures were characterized by means of OM and TEM. Results from DSC and analysis of phase diagram determine solidification paths of *in situ* synthesized Ti6242 composites as following stages: β-Ti primary phase, monovariant binary eutectic β-Ti + TiB, invariant ternary eutectic β-Ti + TiB + TiC and phase transformation from β-Ti to α-Ti. *In situ* synthesized reinforcements are distributed uniformly in titanium matrix alloy. Reinforcement TiB grows in whisker shape whereas TiC grows in globular or near-globular shape. TiB whiskers were made to align the hot-forging direction after hot-forging. The interfaces between reinforcements and Ti matrix alloy are very clean. There is no any interfacial reaction. Moreover, the mechanical properties improved with the addition of TiB whiskers and TiC particles although some reduction in ductility was observed. Fractographic analysis indicated that the composites failed in tension due to reinforcements cracking. The improvements in the composite properties were rationalized using simple micromechanics principles. The strengthening mechanisms are attributed to the following factors: undertaking load of TiB whiskers and TiC particles, high-density dislocations and refinement of titanium matrix alloy's grain size.

1. Introduction

The incorporation of low density, high modulus and high strength reinforcements into titanium, which by itself possesses a high specific strength at room and moderately elevated temperatures, significantly improves its specific modulus, specific strength and creep resistance. According to the shapes of reinforcements, titanium matrix composites (TMCs) can be divided into the following types: TMCs reinforced with continuous fiber, whisker or particle. Compared with TMCs reinforced with continuous fiber, TMCs reinforced with whisker or particle possess isotropic behavior, ease of fabrication and low cost so that TMCs reinforced with whisker or particle have been extensively studied recently.

The TMCs reinforced with whisker or particle are conventionally prepared by powder technology [1, 2] or liquid metallurgy [3, 4], where the ceramic particles are directly incorporated into solid and liquid matrices, respectively. However, titanium metal matrices reinforced with ceramic particles formed *in situ* are an emerging group of discontinuously reinforced composites that have distinct advantages over the conventional TMCs. This process eliminates the interface incompatibility between matrix and reinforcement by creating more thermodynamically stable reinforcements based on their nucleation and growth from parent matrix phase. Thus composites via *in situ* technique demonstrate high specific strength and modulus, as well as excellent oxidation and creep resistance. Self-propagation high-temperature synthesis (SHS) [5, 6], mechanical alloying [7], powder metallurgy [8–11] and rapid solidification processing [12, 13] have been used to produce TMCs by *in situ* technique. Among the several techniques avail to synthesize TMCs, the solidification processes where the reinforcing particles are formed *in situ* in the molten titanium prior to or during its solidification are attractive due to their simplicity, economy and flexibility. The judicious selection of solidification processing techniques, matrix alloy compositions and dispersoids can produce new structures and impart a unique set of useful engineering properties to the composites that are difficult to obtain in conventional monolithic materials.

In the former paper, we highlight a novel *in situ* process in which traditional ingot metallurgy plus SHS technique were used to produce (TiB + TiC)/Ti composites [14]. In this paper, ($TiB_w + TiC_p$)/Ti6242 composites have been fabricated by common casting and hot-forging technology. Microstructure and tensile of properties of *in situ* synthesized ($TiB_w + TiC_p$)/Ti6242 have been discussed.

2. Experimental procedure

2.1. Materials processing

For preparing ($TiB_w + TiC_p$)/Ti MMCs, the raw materials used were two grade sponge titanium, B_4C powder (98%, average particle size: 5–10 μm), aluminum (98%), silicon (99%), zirconium (98.5%) and master alloy of other alloying elements such as Ti-Sn, Ti-Mo. The design alloy composition is Ti-6A1-2Sn-4Zr-2Mo-0.2Si. The volume percentage of reinforcements is 8%. The stoichiometric ratio of sponge titanium, B_4C powder was blended thoroughly, then they were compacted into pellets. The various amounts of pellets along with the sponge titanium and aluminum, silicon, zirconium, Ti-Sn and Ti-Mo were melted homogeneously in a consumable vacuum arc remelting (VAR) furnace. In order to ensure the chemical homogeneity of the composites, the ingots were melted at least three times. The diameter of the ingots is 100 mm. After casting, the ingots were hot-forged into a rod of 20 mm diameter at 1150–1200°C. The total reduction of hot-forging, i.e. A_0/A_i, was 25, where A_0 is the cross section area before hot-forging and A_i is the cross section area after hot-forging. The compositions of the composite are listed in Table I. The oxygen, nitrogen and hydrogen contents in the composite are within the acceptable limits for general titanium alloys.

2.2. Microstructure examination

Samples for optical microscopy (OM) were taken from the products at different stages of processing. Then the samples were prepared using conventional techniques of grinding and mechanical polishing. Lastly, the samples were etched in Kroll's reagent. Phase identification of the composites was performed by a Siemens D-500 X-ray diffractometer. The microstructures were characterized by optical microscopy (OM). A LECO 2000 image analyzer was used to characterize the aspect ratio of TiB whiskers and TiC particles.

The character of reinforcements, finer details of composite microstructure and electron energy-loss spectroscopy (EELS) analyses of reinforcements were carried out using a H800 (200 KV) transmission electron microscope (TEM) equipped with a Gatan666 spectrometer. TEM samples were prepared by the following steps. Firstly, samples were cut from the hot-forging samples along hot-forging direction and cross section. Then, they were thinned down to 100 μm by polishing with SiC paper. At last, they were punched to 3 mm disc samples that were then dimple ground to 20 μm thickness. The final stage of thinning was performed by argon ion milling (Gatan) with an incident angle of 10 deg until perforation occurred.

2.3. Differential scanning calorimeter analysis

In order to investigate the solidification paths, the differential scanning calorimeter (DSC) has been used. DSC analysis was conducted on a Netsch DSC404 instrument. Seventy milligrams of the TMCs were cut from cast sample prepared using the aforementioned method, and the TMCs specimen was then put into an alumina crucible. The alumina crucible that contained the TMCs specimen was placed in the sample cell in the DSC, while an empty alumina crucible was placed in the reference cell. The sample was heated at a rate of 10°C/min from ambient to 1600°C, subsequently cooling to ambient temperature at the same rate, and under dynamic high purity argon atmosphere (80 ml/min). At least three DSC runs were typically made for each sample. All DSC thermograms were normalized to the actual amount of metal (in percentage of weigh) in each sample.

2.4. Mechanical properties evaluation

To study the mechanical properties of composites at ambient temperature under tensile loading, samples of 6 mm gauge diameter and 50 mm length were machined from hot-forging rods with the specimen axis parallel to the hot-forging direction. Three specimens were tested using MTS-810 materials testing machine. The strain rate was 10^{-2} s^{-1}. Load-elongation curves were obtained on an X-Y plotting table that was linked to the load cell of the machine and to an extensometer clamped to test samples. The Young's moduli were determined by measuring the slope of the true stress-true strain curve in the elastic range. The tensile fracture surfaces were investigated by means of a Philips SEM 515.

3. Results and discussion

3.1. Phase identification, microstructure and solidification paths of cast sample

Fig. 1 shows X-ray diffraction patterns for cast sample. It can be concluded that the phases present are Ti, TiB and TiC, namely TiB and TiC reinforced Ti matrix composites can be synthesized by common casting technology utilizing the SHS reaction between Ti and B_4C. The microstructure of cast composites at low magnification and high magnification are shown in Fig. 2a and b respectively. Fig. 2a shows a homogeneous distribution of TiB, TiC reinforcements and confirms that a uniform reinforcement distribution was originally obtained in the cast sample. From Fig. 2b, we can see that *in situ*

TABLE I Chemical composition of titanium matrix composite (wt.%)

Element	Al	Sn	Zr	Mo	Si	B	C	O	N	H	Ti
Amount	5.98	2.03	4.02	1.97	0.09	2.04	0.61	0.075	0.027	0.006	balance

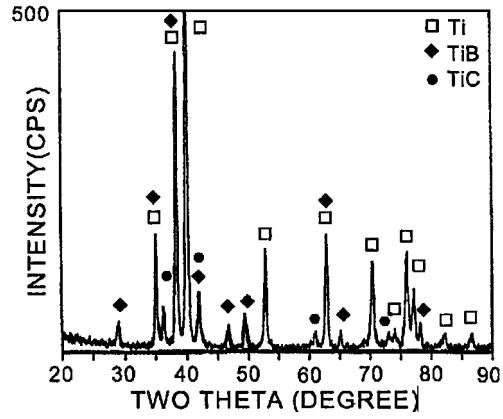

Figure 1 X-ray diffraction patterns for cast sample.

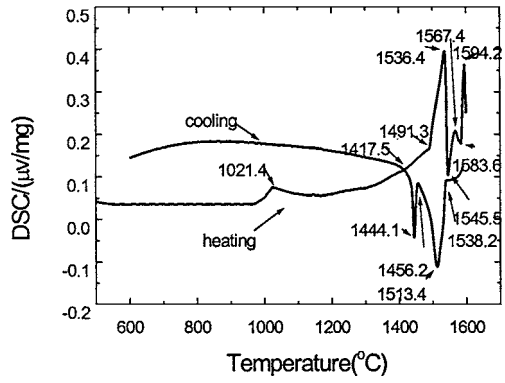

Figure 3 Typical DSC scans for *in situ* synthesized TMCs during heating and cooling procedures.

synthesized reinforcements have two different shapes, i.e. whisker shape and globular or near-globular shape.

Typical DSC traces, which show the solidification and melting paths of TMCs during cooling and heating procedure, are shown in Fig. 3. It can be concluded that there are four endotherm peaks during melting procedure and two exotherm peaks during solidification procedure. During cooling, the peaks of the primary and binary eutectic have been overlapped due to the delay of temperature. The peak of phase transformation from β-Ti to α-Ti is missing. Compared with Ti-B-C liquid project in rich-titanium corner, the addition of alloying elements can't change the solidification path. The solidification path can be expressed as following: firstly, primary β-Ti forms at 1538.2°C. As temperature decreases, TiB and β-Ti binary eutectic would then simultaneously nucleate once the $L \rightarrow TiB + \beta$-Ti monovariant line is met. β-Ti, TiB and TiC would disperse when the $L \rightarrow TiB + TiC + \beta$-Ti ternary eutectic point is met. Lastly, the phase transformation from β-Ti to α-Ti would take place as temperature decreases continuously (about 1021.4°C). Most β-Ti changed into α-Ti. As discussed in paper [14], TiB grows in whisker shape and TiC grows in dendritic or equiaxed, near-equiaxed shape. It is known from solidification paths of *in situ* synthesized (TiB + TiC)/Ti 6242 that it is impossible for eutectic TiC to grow in dendritic shape because there are no composition undercooling. So reinforcements in the composites only show two different shapes, i.e. TiB whisker and TiC particle with globular or near-globular shape, as shown in Fig. 2b.

3.2. Microstructure of hot-forging sample

The microstructure of hot-forging sample also shows a homogeneous distribution of reinforcements. The microstructures of hot-forging sample at longitudinal and transverse cross-sections are shown in Fig. 4a and b, respectively. It can be concluded that the reinforcements are also distributed uniformly in matrix alloy. Compared with microstructure at cast, the TiB whiskers were made to align along the hot-forging direction after hot-forging. The dispersion of reinforcements as viewed at high magnification (Fig. 5) is relatively uniform, showing few clustering. The Ti6242 matrix shows near-equiaxed grains (average size = 15 μm).

The quantitative characterization of reinforcements conducted by a LECO 2000 Image Analyzer reveals that reinforcements have an average aspect ratio (length-to-diameter) 5.42 (as shown in Fig. 6a), ranging from 1 to 20.4. The least percentage of aspect ratio histograms is from 3.0 to 4.0. As shown in Figs 4 and 5, the shape of TiC reinforcement is globular or near-globular, so the reinforcement with aspect ratio less than 3.5 is regarded as TiC, the other is regarded as TiB. The distribution of TiC particles size is mainly ranged from 1.21 to 8.36 μm, have an average particle size 3.46 μm, with average aspect ratio of 1.47. The mean aspect ratio of TiB whiskers is 7.02. The quantitative characterization of reinforcements is shown in Fig. 6b and c. In order to investigate the accuracy of separation between TiB whisker and TiC particle, we have calculated the volume of TiB and TiC using the average size and average aspect ratio. The volume ratio

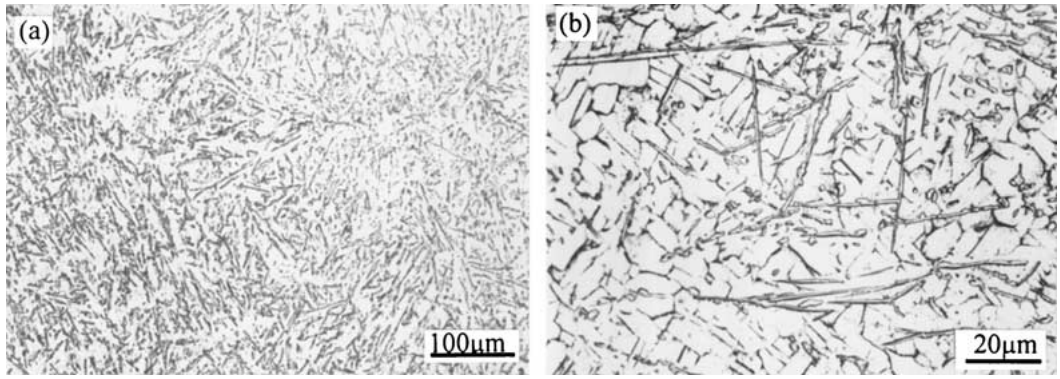

Figure 2 Optical micrographs of cast sample (a) showing the distribution of reinforcements (unetched) (b) showing the different shapes of reinforcements (etched).

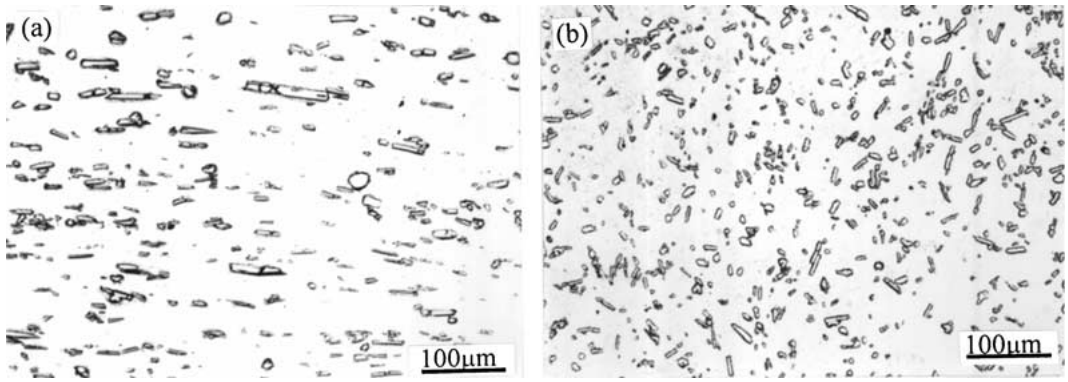

Figure 4 Optical micrographs of hot-forging sample showing the distribution of reinforcements in (a) longitudinal and (b) transverse cross-section (unetched).

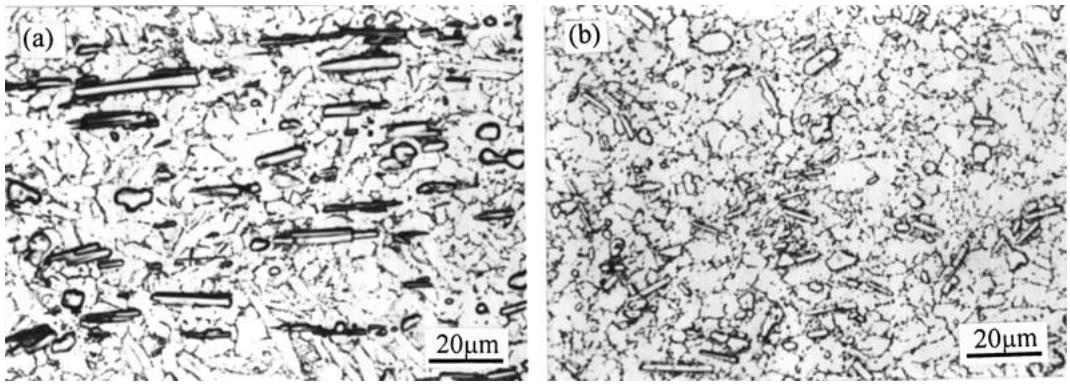

Figure 5 Optical micrographs of hot-forging sample showing the structure of matrix alloy in (a) longitudinal and (b) transverse cross-section (etched).

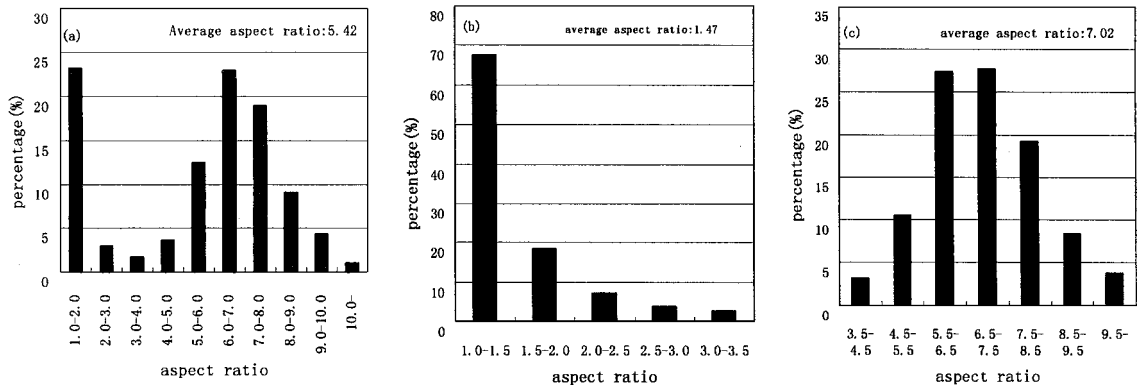

Figure 6 Quantitative analysis of aspect ratio histograms of (a) reinforcements (b) TiC (c) TiB.

between TiB and TiC is 4.18, which is close to the designed volume ratio between TiB and TiC of 4.35. So it is reasonable to separate TiB whiskers and TiC particles at the point of 3.5. Moreover, the average aspect ratio of 1.47 is close to the results of TiC *in situ* synthesized by vacuum melting which shows that the aspect ratio of TiC ranges from 1 to 3.5, with an average aspect ratio of 1.49 [15].

TEM examination of as-fabricated composite indicates that the TiB whiskers are generally polygonal and faceted. It is different in TiB shape at transverse cross-section and longitudinal cross-section. The TEM bright field images of TiB at transverse and longitudinal cross-section are shown in Fig. 7a and b. Fig. 7c and d are the respective selected area diffraction of TiB. We can also conclude that the interface between TiB and titanium matrix alloy is clean. Fig. 7e shows EELS analysis results of TiB whiskers, exhibiting an atomic composition of TiB. The mole ratio between Ti atom and B atom is 1 : 1.

Fig. 8 shows an individual particle of TiC in the composite. It can be seen that the interface between TiC and matrix alloy is also clean. There is no any interfacial reaction. Fig. 8b shows a SAD of TiC in [110] direction, with face-centered cubic crystal structure having a lattice parameter of 0.431 nm. Fig. 8c shows EELS analysis results of TiC particles, exhibiting an atomic composition of $TiC_{0.8}$. The mole ratio between Ti atom and C atom is 5 : 4. Fig. 9 shows a TEM image of titanium matrix alloy. There are high-density dislocations in matrix alloy. The high-density dislocations will improve the mechanical properties of matrix alloy.

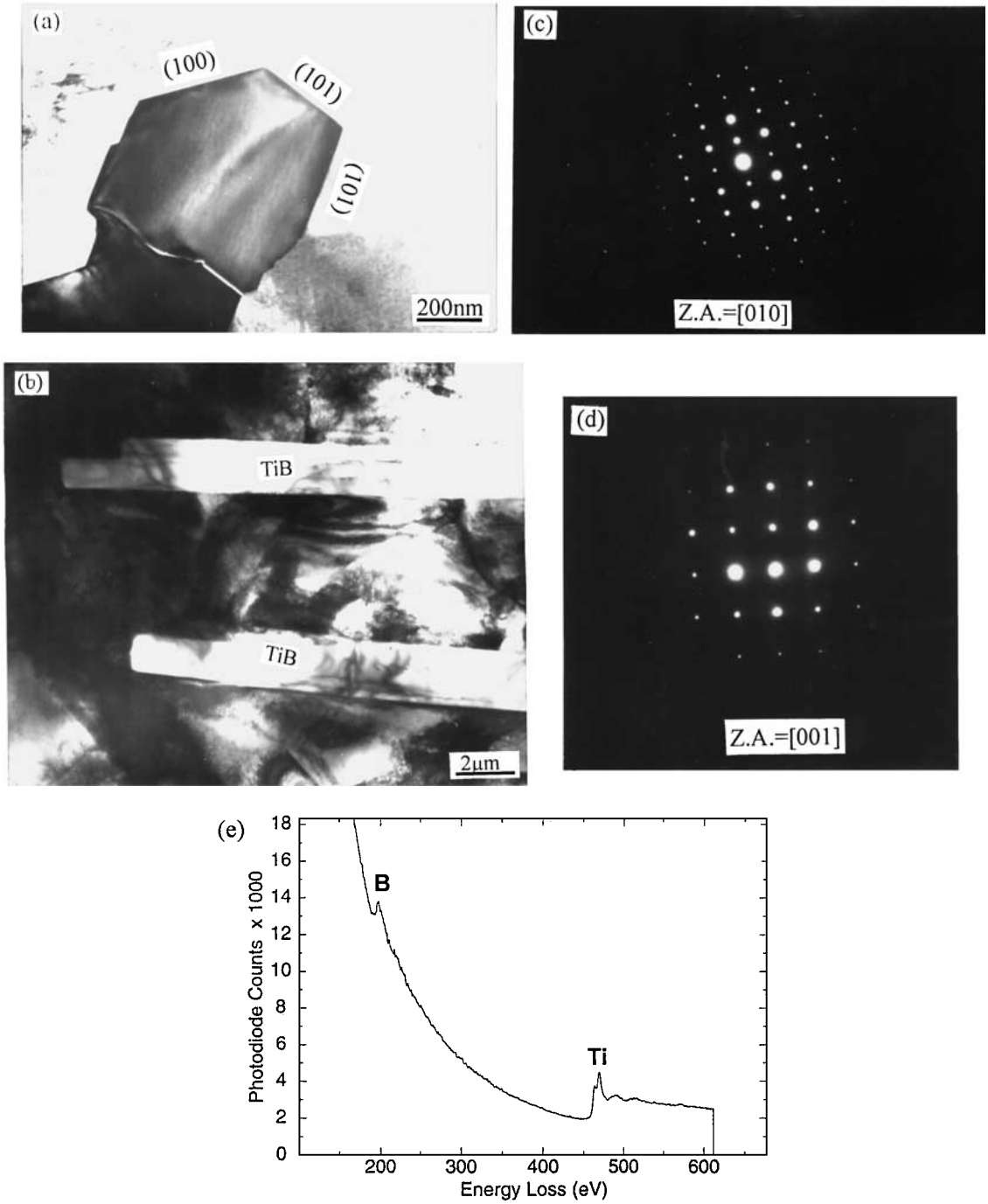

Figure 7 TEM images of TiB whiskers in hot-forging sample. (a) and (b) are transverse and longitudinal views, accompanied by their respective SAD in (c) and (d), (e) EELS pattern of TiB. Note the correspondence between the crystallographic facets of the TiB.

TABLE II Mechanical properties of *in situ* synthesized (TiB + TiC)/Ti composites and matrix alloy

Specimen	E (GPa)	Y.S. (MPa)	U.T.S (MPa)	Elongation (%)	E^a (GPa)	Y.S.[a] (MPa)	E^b (GPa)
Ti6242	110	844	914	10			
Ti MMCs	130.5	1160.6	1234.0	1.35	132.7	1050.0	139.0

where a points the theoretic values which are calculated by micromechanism, while b points the theoretic value calculated by the rule of mixture.

3.3. Mechanical properties

The mechanical properties measured by tensile testing are listed in Table II and compared to matrix alloy Ti6242. These results indicate that the Young's modulus increases with the addition of *in situ* synthesized TiB and TiC reinforcements. The rule of mixtures can not be applied to determine the elastic modulus of such composites because it is only valid for composites reinforced with continuous fibres. However the elastic modulus of discontinuously reinforced composites E_c can be estimated using the Tsai-Halpin equation [16]:

$$E_c = \frac{E_m(1 + 2s \cdot qV_p)}{1 - qV_p} \quad (1)$$

The parameter q is given by the following equation:

$$q = \frac{(E_p/E_m - 1)}{(E_p/E_m + 2s)} \quad (2)$$

where E_m and E_p are the Young's moduli of the matrix and reinforcements such as TiB whiskers and TiC

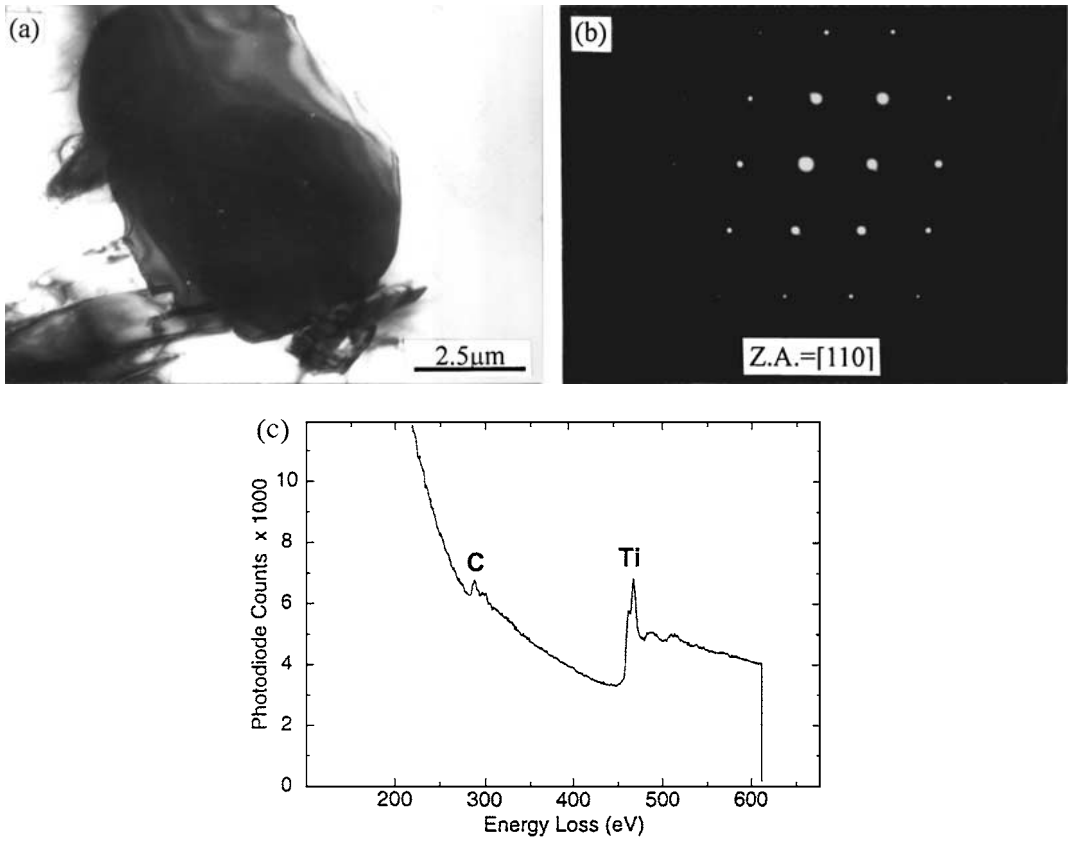

Figure 8 (a) TEM microstructure of TiC in the composite (b) SAD of TiC (c) EELS pattern of TiC.

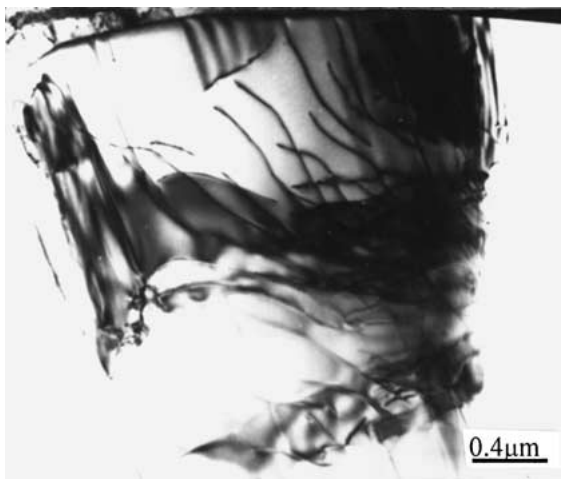

Figure 9 TEM image of titanium matrix alloy which shows the high-density dislocations.

particles, respectively, V_p is the reinforcements volume fractions of TiB whiskers and TiC particles in the composites and s is the aspect ratio of reinforcement. Young's moduli of TiB whiskers, TiC particles and the matrix introduced in calculations are $E_{TiB} = 480$ GPa, $E_{TiC} = 440$ GPa and $E_{matrix} = 110$ GPa. The predicted elastic modulus of composites is also listed in Table II using the average aspect ratio of reinforcements in the former part. The elastic modulus estimated from the rule of mixtures (isostrain condition) is also shown only for comparison purposes. The experimental values appear to well fit the Tsai-Halpin equation.

Yield strength and ultimate tensile strength are also improved due to the addition of *in situ* synthesized TiB and TiC reinforcements (Table II). The effect of TiB whisker and TiC particle reinforcements on composite strength can be rationalized using existing micromechanics models. According to Kelly's theory [17], there exists a critical whisker aspect ratio, e.g. those whiskers whose aspect ratios exceed the critical whisker aspect ratio play an important role in strengthening. Generally, the critical whisker aspect ratio l_c/d can be expressed by Kelly's equation:

$$\frac{l_c}{d} = \frac{\sigma_f}{2\tau_i} \tag{3}$$

where l_c, d, τ_i and σ_f are the fiber critical length, fiber diameter, the shear strength of the interface and shear strength of whiskers. Assuming that the interfacial bond is strong enough, τ_i will be limited by the shear strength of the matrix (τ_m):

$$\tau_i = \tau_m \tag{4}$$

The values of τ_m and σ_f are set equal to σ_{ym} of titanium matrix alloy (844 MPa) and TiB whiskers (3500 MPa) respectively. Thus,

$$\frac{l_c}{d} = \frac{\sigma_f}{2\sigma_{ym}} = 2.07$$

Moreover, the mean whisker aspect ratio is 7.02, which is bigger than the critical value. It indicates that the *in situ* synthesized TiB whiskers play an important role in strengthening. It can be confirmed by the fracture micrograph (as shown in Fig. 10) that shows the fracture surface of the hot-forging materials tested under tension at ambient temperature. This exhibits a predominantly brittle cleavage fracture mechanism. In

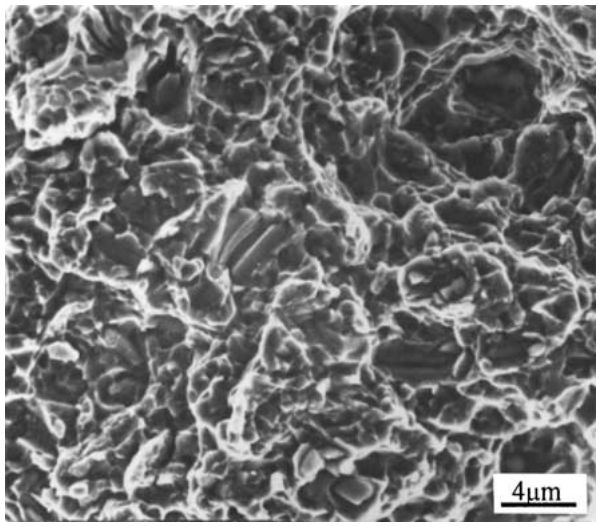

Figure 10 Fractography of 8 vol% (TiB + TiC)/Ti composite after tensile test.

most instances the crack passes through the reinforcements and fractures them. It is also well known that oxygen and nitrogen reduce significantly the ductility of titanium alloys. However, considering the fact that the contents in the matrix alloy of impurity such as oxygen and nitrogen are within the acceptable limits for general titanium alloys, an embrittlement of the matrix caused during the production can be excluded. So the low ductility of the composite is attributed to reinforcements cracking. Moreover, there is no decohesion and interface separation between reinforcements and titanium matrix alloy. All of these indicate that the interface cohesion between reinforcements and titanium matrix alloy is strong enough and the reinforcements can undertake load and improve mechanical properties.

A shear-lag model, developed by Cox [18] and modified by Nardone and Prewo [19, 20], was used to calculate the yield stress of composites reinforced with short-oriented whiskers and particles accounting for load transfer at whisker and particle ends. For composites reinforced with short-oriented whiskers and particles, the yield stress of the composite σ_{yc} are shown as Equations 5 and 6, respectively:

$$\sigma_{yc}/\sigma_{ym} = 0.5V_W(2 + l/d) + (1 - V_W) \quad (5)$$

$$\sigma_{yc} = \sigma_{ym}V_p\left[1 + \frac{(L + t)A}{4L}\right] + \sigma_{ym}(1 - V_p) \quad (6)$$

where σ_{ym} is the yield stress of the titanium matrix alloy, V_w is the whisker volume fraction, l/d is the whisker aspect ratio, L is the length of the particle perpendicular to the applied stress, A is the particle-aspect ratio, V_p is the particle volume fraction.

Considering the effects of TiB whiskers and TiC particles, the increase of yield stress $\Delta\sigma$ can be expressed as following:

$$\Delta\sigma = \sigma_{ym}\left[0.5V_W \cdot l/d + V_p \cdot \frac{(L + t)A}{4L}\right] \quad (7)$$

Assuming the TiB whisker and TiC particle align forging direction perfectly, the calculated increase of yield stress $\Delta\sigma/\sigma_{ym}$ is 24.2%, i.e. the yield stress of composites is about 1050 MPa. It can be concluded from the calculation that the theoretical value is less than the measured value. The discrepancy may be attributed to various factors not included in this model. In Equations 5–7, the strengthening effect of titanium alloy matrix, which results from the refine of grain size is not included. According to Hall-Petch relationship [21], the strengthening effect is in proportion to $d^{-1/2}$ (d, grain size):

$$\sigma_y = \sigma_0 + K_y d^{\frac{1}{2}} \quad (8)$$

Typically σ_0 is rationalized as either a frictional stress resisting the motion of gliding dislocations or as an internal back stress. K_y is the Hall-Petch slope, which is considered to be a measurement of the resistance of the grain boundary to slip transfer. It can be seen from Fig. 6 that the grain size is very fine. In fact, the existing of reinforcements TiB and TiC with high melt point results in the refinement of grain size. From Equation 8, we can know that the decrease in the grain size will increase the yield stress of matrix alloy. Moreover, the high-density dislocations that exist in titanium matrix alloy also improve the strength of TMCs. So we can conclude that the strengthening mechanisms of the composite mainly come from the following factors: (1) undertaking load of reinforcements including TiB whiskers and TiC particles, (2) refinement of titanium matrix alloy's grain size, (3) intrinsic strengthening of high-density dislocations in the matrix alloy.

4. Conclusions

From the results of the present investigation, it can be concluded that ($TiB_w + TiC_p$)/Ti6242 composites can be produced by common casting technique utilizing the SHS reactions between titanium and B_4C. The reinforcements TiB and TiC are distributed uniformly in the titanium matrix. Results from DSC and the analysis of the phase diagram determine solidification paths of *in situ* synthesized Ti6242 composites as following stages: β-Ti primary phase, monovariant binary eutectic β-Ti + TiB, invariant ternary eutectic β-Ti + TiB + TiC and phase transformation from β-Ti to α-Ti. The reinforcement TiB grows in whisker shape whereas the TiC grows in globular or near-globular shape during solidification. TiB whiskers are made to align in parallel to the hot-forging direction. The interfaces between TiB, TiC and titanium matrix alloys are very clean. There is no any interfacial reaction and the bond strength is very strong.

The incorporation of TiB whiskers and TiC particles improves the strength and the Young's modulus. However, the ductility of composites decreases. The Young's modulus is in good agreement with that calculated from the Tsai-Halpin equation applied for discontinuous composites. The tensile yield strength of the composites was compared to the Nardone and Prewo model. The experimental values of yield strength are less than the theoretical values. The strengthening mechanisms

of the composite mainly include the following factors: undertaking load of reinforcements including TiB whiskers and TiC particles, refinement of titanium matrix alloy's grain size, and intrinsic strengthening of high-density dislocations in the matrix alloy.

Acknowledgements

We would like to acknowledge the finance support provided by the National Science Foundation of People's Republic of China under the Grant No: 59631080 and the support of Shanghai New Materials Center.

References

1. P. WANJARA, S. YUE, R. A. L. DREW, J. ROOT and R. DONABERGER, *Key Eng. Mater.* **127–131** (1997) 415.
2. S. ABKOWITZ and S. M. ABKOWITZ, *Industrial Heating* **60**(9) (1993) 32.
3. Y. LIN, R. H. ZEE and A. CHIN, *Metall. Trans. A* **22** (1991) 859.
4. R. ZEE, C. YANG, Y. X. LIN and B. CHIN, *J. Mater. Sci.* **26** (1991) 3853.
5. H. T. TSANG, C. G. CHAO and C. Y. MA, *Scripta Metall. Mater.* **37** (1997) 1359.
6. S. RANGNATH, M. VIJAYAKUMAR and J. SUBRAHMANYAM, *Mater. Sci. Eng. A* **149** (1992) 253.
7. TERUO TAKAHASHI, *J. Japan. Inst. Metals* **59** (1995) 244 (in Japanese).
8. J. Q. JIANG, T. S. LIM, Y. J. KIM, B. K. KIM and H. S. CHUNG, *Mater. Sci. Tech.* **12** (1996) 362.
9. Z. FAN, H. J. NIU, A. P. MIODOWNIK, T. SAITO and B. CANTOR, *Key Eng. Mater.* **127–131** (1997) 423.
10. T. SAITO, H. TAKAMIYA and T. FURUTA, *Mater. Sci. Eng. A* **243** (1998) 273.
11. M. KOBAYASHI, K. FUNAMI, S. SUZUKI and C. OUCHI, *ibid.* **243** (1998) 279.
12. W. O. SOBOYEJO, R. J. LEDERICH and S. M. L. SASTRY, *Acta Metall. Mater.* **42** (1994) 2579.
13. S. DUBEY, R. J. LEDERICH and W. O. SOBOYEJO, *Metall. Mater. Trans. A* **28** (1997) 2037.
14. X. N. ZHANG, W. J. LU, D. ZHANG, R. J. WU, Y. J. BIAN and P. W. FANG, *Scripta Metall. Mater.* **41** (1999) 39.
15. H. T. TSANG, C. G. CHAO and C. Y. MA, *ibid.* **35** (1996) 1007.
16. J. C. HALPIN, "Premer on Composite Materials Analysis" 2nd ed. (Technomic Publ. Co., Lancaster, 1992).
17. A. KELLY and W. R. TYSON, *J. Mech. Phy. Solids* **13** (1965) 329.
18. H. L. COX, *Br. J. Appl. Phys.* **3** (1952) 72.
19. V. C. NORDONE and K. M. PREWO, *Scripta Metall. Mater.* **20** (1986) 43.
20. V. C. NORDONE, *ibid.* **21** (1987) 1313.
21. R. J. MCELROY and Z. C. SZKOPIAK, *Int. Met. Rev.* **17** (1972) 175.

Received 1 June 2000
and accepted 16 January 2001